Combined CDF and DØ upper limits on MSSM Higgs boson production in tau-tau final states with up to 2.2 fb^{-1} of data

The TEVNPH Working Group*

for the CDF and DØ Collaborations

August 15, 2009

Combined results are presented on the search for a neutral Higgs Boson in the di-tau final state using 1.8 fb^{-1} and 2.2 fb^{-1} of integrated luminosity collected at the CDF and DØ experiments respectively. Data were collected in $p\bar{p}$ collisions at a centre of mass energy of 1.96 TeV during RunII of the Tevatron. Limits are set on the cross section $\times$ branching ratio of $H \to \tau\tau$ ranging from 17.2 pb to 0.669 pb for Higgs masses from 100 GeV to 200 GeV respectively. The results are then interpreted as limits in the $\tan\beta$-M_A plane in four different benchmark scenarios within the framework of the MSSM.

Preliminary Results

I.   INTRODUCTION

Spontaneous symmetry breaking in the electroweak sector is an attractive solution to the problem of the origin of particle masses within the Standard Model (SM). However, extreme fine tuning is required to avoid divergences in radiative corrections to the Higgs mass. Supersymmetry (SUSY) as an extension to the SM, provides a natural means to avoid this as well as potentially providing a candidate for dark matter and GUT-scale unification. The Minimal Supersymmetric Standard Model (MSSM) [1] requires the introduction of two Higgs doublets and predicts the existence of five physical Higgs bosons after symmetry breaking: three neutral (h, H, and A) and two charged $H^{\pm}$. The ratio of the vacuum expectation values of the two doublets is denoted $\tan\beta$. For high values of $\tan\beta$ two of the three neutral Higgs bosons have approximately the same mass and couplings - these are enhanced with respect to the charged leptons and down-type quarks - by a factor $\tan\beta$ relative to the SM - and suppressed for the neutrinos and up-type quarks. The near degeneracy contributes an additional factor two enhancement in the cross section. Thus for low M_A and high $\tan\beta$ the Tevatron can probe a number of benchmark scenarios in the MSSM complementing the regions probed by the LEP experiments[2].

II.   ANALYSIS SUMMARY

The CDF and DØ detectors are described in detail elsewhere [3, 4]. The searches combined here are described in detail in [5–7] and earlier published results from CDF and DØ can be found in [9, 10].

Searches are performed at CDF and DØ for MSSM Higgs boson production with subsequent decays to taus in a number of channels characterised by the eventual decay products of the τ leptons. Included in this combination are 1.8 fb^{-1} of data collected at CDF from RunIIa and RunIIb in three final states: $\tau_e\tau_{\mathrm{had}}$, $\tau_\mu\tau_{\mathrm{had}}$ and $\tau_e\tau_\mu$, (where τ_e, τ_μ, and τ_{had} denote τ decays to electron, muon and hadrons respectively) and 1.0 fb^{-1} from RunIIa in the same three channels and 1.2 fb^{-1} from RunIIb in the $\tau_\mu\tau_{\mathrm{had}}$ final state collected at DØ . Additionally, the searches from DØ are split further depending on the hadronic decay mode.

A.   Lepton Identification

Electrons are identified through their characteristic energy deposits in the calorimeters. Reconstructed clusters of energy in the calorimeter are required to be isolated and match a reconstructed track, suppressing photon backgrounds. Muons are identified by matching charged tracks in the central tracking detectors with hits in the muon detectors. Muon candidates are also required to be isolated in both the central tracking detectors and in the calorimetry.

Hadronic decays of τ leptons are identified at CDF by selecting isolated narrow clusters in the calorimeter with 1 or 3 spatially matched charged tracks. These are reconstructed using a variable sized cone algorithm whose angle, α, is set to be the minimum of $10°$ and $(5 \text{ GeV})/E_{cl}$ radians, where E_{cl} is the calorimeter cluster energy. Strict isolation limits on the number of tracks and the calorimeter energy within an annulus around the candidate from α out to an angle of $30°$ are used to suppress quark and gluon jets. In the case of 3-prong candidates the sum of the charges of the tracks is required to be ±1. 1-prong candidates are rejected if found to be consistent with an electron having undergone significant bremsstrahlung.

In the DØ analyses, the hadronic decays of the τ into three categories: τ-types 1 and 2 are 1-prong candidates with energy either in only the hadron calorimeter ($\pi^{\pm}$ like) or in both the electromagnetic and hadron calorimeters ($\rho^{\pm}$ like) respectively; τ-type 3 is a 3-prong candidate with an invariant mass (constructed from the three tracks) below 1.7 GeV and matching energy deposits in the calorimeters. A neural network (NN) is trained for each type to separate hadronic tau decays from jets using MC $Z \to \tau\tau$ as the signal and multi-jet events taken from data as the background. An additional NN is trained on electron Monte-Carlo events and is employed to reduce backgrounds from electrons faking type 2 taus.

B.   Signal, Backgrounds and Event Selection

The acceptance for signal is determined from Monte-Carlo simulations, using the PYTHIA[11] event generator with CTEQ5L (CDF) and CTEQ6L [12] (DØ) parton sets and TAUOLA[13] to simulate the decays of the final state τ-leptons. The response of the detectors is modelled using GEANT[15] based simulations. Two production modes, $gg \rightarrow \phi$ and $b\bar{b}\phi$ are considered by CDF, whereas at DØ only $gg \rightarrow \phi$ is simulated - the acceptances are seen to be very similar for both production modes. In the interpretation of the results in the framework of the MSSM as limits in the $\tan\beta$-M_A plane both production modes are taken into account as well as an additional factor of two on the cross section due to the near degeneracy of two of the three neutral Higgs bosons. Most Standard Model backgrounds have been generated with PYTHIA: $Z\gamma^* \rightarrow l^+l^-$, $W \rightarrow l\nu$, di-boson production, $t\bar{t}$ (COMPHEP + PYTHIA)[14]. W and Z boson samples where there is one or more additional jets in the final state have been simulated with ALPGEN with matching to PYTHIA for hadronization. Di-boson and $t\bar{t}$ samples are normalised using calculations to next-to-LO (NLO) while Z/γ^* samples are generally normalised to next-to-NLO (NNLO).

Events are selected by the trigger using inclusive electron and muon (DØ) and lepton plus track (CDF) triggers and after offline reconstruction candidate events must contain two isolated opposite charged final state leptons (e, μ, τ). Leading sources of background are: $Z/\gamma^* \rightarrow \tau\tau$, multi-jet, $W \rightarrow e\nu, \mu\nu, \tau\nu$, $Z \rightarrow \mu\mu, Z \rightarrow ee$, di-boson $(WW, WZ, ZZ, W\gamma, Z\gamma)$, and $t\bar{t}$-pair production. In the $\tau_e\tau_\mu$ channel at CDF, events from the sidebands of the lepton isolation are used to determine the jet backgrounds. For the $\tau_e\tau_{\rm had}$ and $\tau_\mu\tau_{\rm had}$ channels the jet backgrounds where a jet fakes a $\tau_{\rm had}$ are estimated by weighting data events passing very loose cuts with the jet-*tau* fake probability measured in an independent jet sample. The multi-jet contribution from data collected at DØ is estimated using either $\tau_e\tau_{\rm had}$ candidate events where the electron and τ have the same charge or using inverted lepton selection criteria ($\tau_\mu\tau_{\rm had}$ and $\tau_e\tau_\mu$ channels). The normalisation of the W production backgrounds is estimated from a data sample dominated by W+jet events.

In the $\tau_e\tau_{\rm had}$ and $\tau_\mu\tau_{\rm had}$ channels the electron or muon are required to be isolated and have a transverse momentum, $p_T > 10$ (CDF) or 15 (DØ) GeV. 1-prong hadronic tau candidates are accepted with $p_T > 15$ GeV (CDF), 16.5 GeV (DØ) and 3-prong are required to have $p_T > 20$ GeV (CDF) 22 GeV (DØ). Additional cuts are placed on the scalar sum of transverse momenta in the event at CDF, $H_T = |p_T^{e/\mu}| + |p_T\tau_{\rm had}| + |\not{E}_T| > 55$ GeV. In 1-prong events where the rate at which jets fake taus is lower a slightly looser cut is used, $H_T > 50$ or 45 GeV for $\tau_e\tau_{\rm had}$ and $\tau_\mu\tau_{\rm had}$ respectively. Further cuts on the relative directions of the taus and the $\not{E}_T$(CDF and DØ) and the transverse mass (DØ) $M_T = \sqrt{2p_T^{e/\mu}\not{E}_T(1 - \cos\Delta\phi)}$, where $\Delta\phi$ is the azimuthal angle between the electron or muon and the hadronic tau, serve to suppress background contributions from W+jets production.

In the CDF $\tau_e\tau_\mu$ channel events are selected requiring one central electron and one central muon with: $\min(E_T^e, p_T^\mu) > 6$ GeV, $\max(E_T^e, p_T^\mu) > 10$ GeV, and $|E_T^e| + |p_T^\mu| > 30$ GeV. DØ make a similar selection, where: $p_T^\mu > 10$ GeV and $p_T^e > 12$ GeV and the invariant mass of the electron-muon pair exceeds 20 GeV and $|E_T^e| + |p_T^\mu| + |\not{E}_T| > 65$ GeV. Table I shows the expected number of backgrounds, observed events in data and the signal efficiency for $M_A = 130$ GeV.

In setting the limits, events from regions of phase-space with a similar ratio of expected signal (S) to background (B) can be combined without loss of sensitivity. Thus a useful way to visualize the comparison of expected backgrounds and the observed data is to show the event distributions binned in this ratio S/B. For the channels combined in the results presented in this note these distributions are shown in Figure 1. The left hand plot is for a signal, $M_A = 100$ GeV and $\sigma \times$Br= 2.0pb and the right hand plot for a signal of $M_A = 180$ GeV and $\sigma \times$ Br=0.66pb. Good agreement is observed between the data and expected backgrounds. The integrals of these distributions starting from the high S/B side and working downwards are shown in Figure 2, displaying the signal+background, background-only and data sums.

III.   COMBINATION

To gain confidence that the final result does not depend on the details of the statistical formulation, two types of combinations are performed, using the Bayesian and Modified Frequentist approaches, which give similar results (within 10%). Both methods rely on distributions in the final discriminants, and not just on their single integrated

Source	CDF			DØ		
	$\tau_e\tau_\mu$	$\tau_e\tau_{\text{had}}$	$\tau_\mu\tau_{\text{had}}$	$\tau_e\tau_\mu$	$\tau_e\tau_{\text{had}}$	$\tau_\mu\tau_{\text{had}}$
$Z \to \tau\tau$	605 ± 51	1378 ± 117	1353 ± 116	212 ± 3	581 ± 5	2160 ± 33
$Z \to e^+e^-/Z \to \mu^+\mu^-$	19.4 ± 5.7	70 ± 10	107 ± 13	10.4 ± 0.9	31 ± 2	67 ± 6
diboson $+ t\bar{t}$	20.5 ± 7.0	8.2 ± 4.2	6.6 ± 3.7	6.1 ± 0.1	3.0 ± 0.1	15.7 ± 2.6
multi-jet $+ W \to l\nu$	57.1 ± 13.5	467 ± 73	285 ± 46	37.9 ± 2.4	386 ± 21	217 ± 11
Total Background	702 ± 55	1922 ± 141	1752 ± 129	266 ± 4	989 ± 22	2459 ± 36
Data	726	1979	1666	274	1034	2340
Signal Efficiency /%	0.32 ± 0.01	0.77 ± 0.01	0.67 ± 0.01	0.41 ± 0.03	0.73 ± 0.03	0.99 ± 0.05

TABLE I: Expected numbers of background and observed data events and signal efficiency for $M_A = 130$ GeV. Errors shown are statistical only.
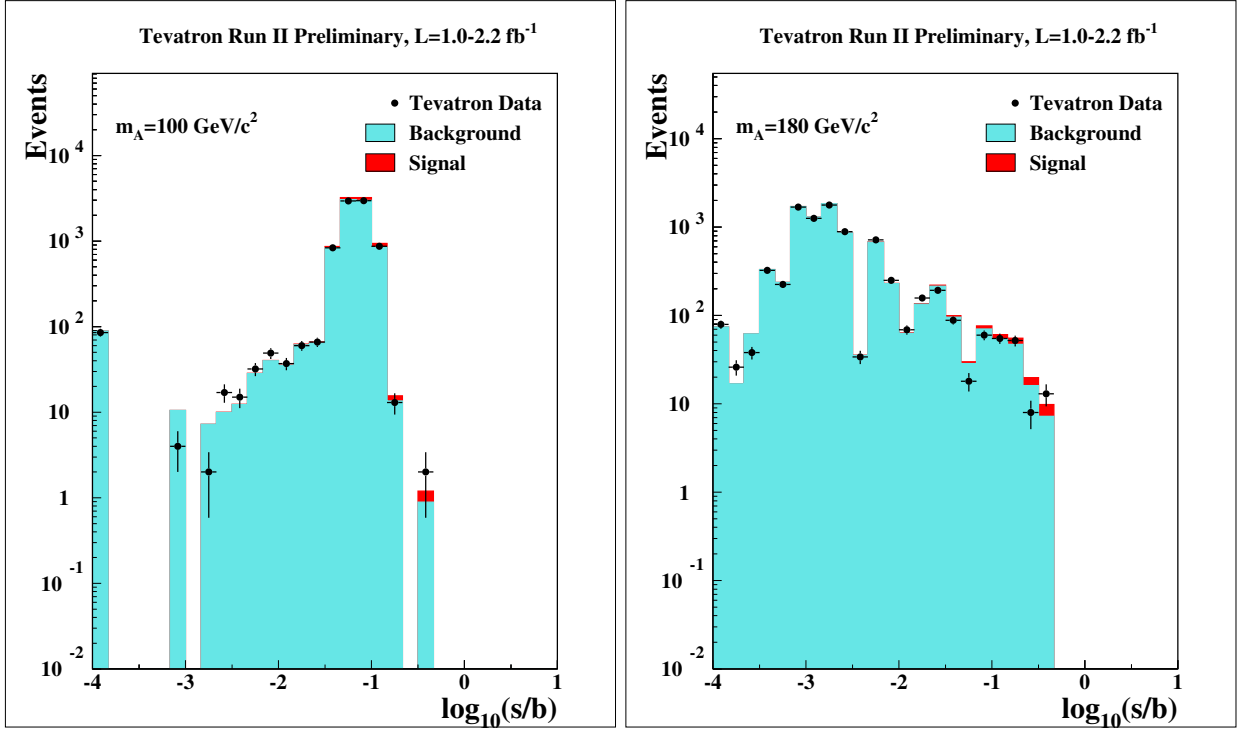

FIG. 1: Events binned by the ratio of expected signal to expected background for a signal of $M_A = 100$ GeV, and $\sigma \times \text{Br} = 2.0$pb (left) and $M_A = 180$ GeV, and $\sigma \times \text{Br} = 0.66$pb (right)

values. Systematic uncertainties enter as uncertainties on the expected number of signal and background events, as well as on the distribution of the discriminants in each analysis ("shape uncertainties"). Both methods use likelihood calculations based on Poisson probabilities. In all channels the visible mass distribution is used to set limits.

A. Bayesian Method

Because there is no experimental information on the production cross section for the Higgs boson, in the Bayesian technique [17] a flat prior is assigned for the total number of selected Higgs events. For a given Higgs boson mass, the
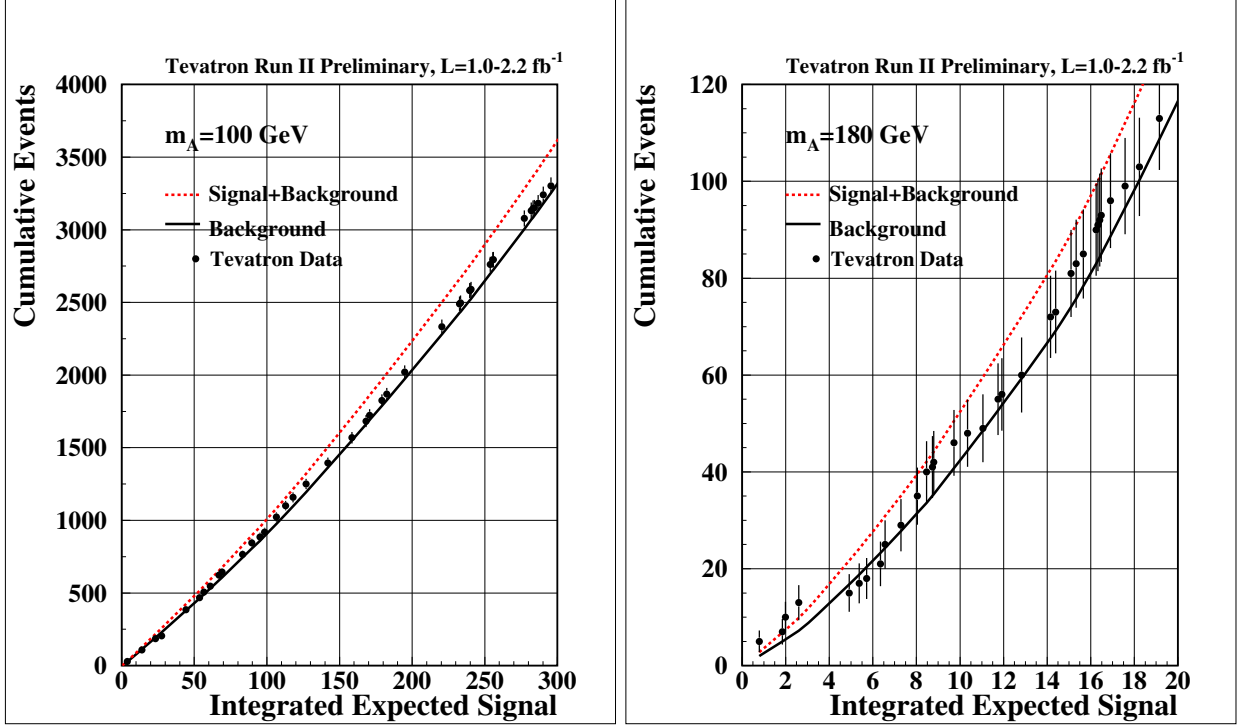
FIG. 2: Integrated distributions of S/B, starting at the high S/B side for $M_A = 100$ GeV, $\sigma \times$Br= 2.0pb (left) and $M_A = 180$ GeV, $\sigma \times$ Br=0.66pb (right). The total signal+background and background-only integrals are shown separately with data superimposed. Data points are only plotted for those bins with data events.

combined likelihood is a product of likelihoods for the individual channels, each of which is a product over histogram bins:

$$\mathcal{L}(R, \vec{s}, \vec{b} | \vec{n}, \vec{\theta}) \times \pi(\vec{\theta}) = \prod_{i=1}^{N_C} \prod_{j=1}^{Nbins} \mu_{ij}^{n_{ij}} e^{-\mu_{ij}} / n_{ij}! \times \prod_{k=1}^{n_{np}} e^{-\theta_k^2/2} \tag{1}$$

where the first product is over the number of channels (N_C), and the second product is over histogram bins containing n_{ij} events, binned in ranges of the final discriminants used for individual analyses, such as the di-jet mass, neural-network outputs, or matrix-element likelihoods. The parameters that contribute to the expected bin contents are $\mu_{ij} = R \times s_{ij}(\vec{\theta}) + b_{ij}(\vec{\theta})$ for the channel i and the histogram bin j, where s_{ij} and b_{ij} represent the expected background and signal in the bin, and R is a scaling factor applied to the signal to test the sensitivity level of the experiment. Truncated Gaussian priors are used for each of the nuisance parameters θ_k, which define the sensitivity of the predicted signal and background estimates to systematic uncertainties. These can take the form of uncertainties on overall rates, as well as the shapes of the distributions used for combination. These systematic uncertainties can be far larger than the expected Higgs signal, and are therefore important in the calculation of limits. The truncation is applied so that no prediction of any signal or background in any bin is negative. The posterior density function is then integrated over all parameters (including correlations) except for R, and a 95% credibility level upper limit on R is estimated by calculating the value of R that corresponds to 95% of the area of the resulting distribution.

B. Modified Frequentist Method

The Modified Frequentist technique relies on the CL_s method, using a log-likelihood ratio (LLR) as test statistic [18]:

$$LLR = -2 \ln \frac{p(\text{data}|H_1)}{p(\text{data}|H_0)}, \tag{2}$$

where H_1 denotes the test hypothesis, which admits the presence of SM backgrounds and a Higgs boson signal, while H_0 is the null hypothesis, for only SM backgrounds. The probabilities p are computed using the best-fit values of the nuisance parameters for each event, separately for each of the two hypotheses, and include the Poisson probabilities of observing the data multiplied by Gaussian constraints for the values of the nuisance parameters. This technique extends the LEP procedure which does not involve a fit, in order to yield better sensitivity when expected signals are small and systematic uncertainties on backgrounds are large [20].

The CL_s technique involves computing two p-values, CL_{s+b} and CL_b. The latter is defined by

$$1 - CL_b = p(LLR \leq LLR_{\text{obs}}|H_0), \tag{3}$$

where LLR_{obs} is the value of the test statistic computed for the data. $1 - CL_b$ is the probability of observing a signal-plus-background-like outcome without the presence of signal, i.e. the probability that an upward fluctuation of the background provides a signal-plus-background-like response as observed in data. The other p-value is defined by

$$CL_{s+b} = p(LLR \geq LLR_{\text{obs}}|H_1), \tag{4}$$

and this corresponds to the probability of a downward fluctuation of the sum of signal and background in the data. A small value of CL_{s+b} reflects inconsistency with H_1. It is also possible to have a downward fluctuation in data even in the absence of any signal, and a small value of CL_{s+b} is possible even if the expected signal is so small that it cannot be tested with the experiment. To minimize the possibility of excluding a signal to which there is insufficient sensitivity (an outcome expected 5% of the time at the 95% C.L., for full coverage), we use the quantity $CL_s = CL_{s+b}/CL_b$. If $CL_s < 0.05$ for a particular choice of H_1, that hypothesis is deemed excluded at the 95% C.L.

Systematic uncertainties are included by fluctuating the predictions for signal and background rates in each bin of each histogram in a correlated way when generating the pseudo-experiments used to compute CL_{s+b} and CL_b.

C. Systematic Uncertainties

The uncertainty on the measurement of the integrated luminosity is 6% (CDF) and 6.1% (DØ). Of this value, 4% arises from the uncertainty on the inelastic $p\bar{p}$ scattering cross section, which is correlated between CDF and DØ. The uncertainty on the rates for $t\bar{t}$ production and for single and di-electroweak boson production are taken as correlated between the two experiments. As the methods of measuring the multi-jet ("QCD") backgrounds differ between CDF and DØ, there is no correlation assumed between these rates. The calibrations of fake leptons, unvetoed $\gamma \rightarrow e^+e^-$ conversions, b-tag efficiencies and mistag rates are performed by each collaboration using independent data samples and methods, hence are considered uncorrelated.

Tables II to VIII summarize the various contributions to the systematics uncertainties to the input distributions used in the limit setting, broken down by experiment and channel. Entries in the tables labeled as "shape" systematics do not have the same value across all bins of the relevant distribution and model the systematic variation of the shape for that source of uncertainty. In these cases the number given is the event weighted mean fluctuation away from the nominal distribution - i.e. related to the flat component of the uncertainty.

Contribution	Signal	$Z \to e^+e^-$	$Z \to \tau\tau$	$t\bar{t}$	diboson	QCD
Jet energy scale (shape)	0.12	$+0.30$ $+0.22$	$+0.05$ 0.00	0.56	0.73	0.0
Electron identification	2.4	2.4	2.4	2.4	2.4	0.0
Electron energy scale (shape)	$+0.32$ -0.23	0.00 $+0.30$	$+0.77$ -0.50	-0.19 $+0.28$	-0.09 $+0.16$	0.0
Tau identification	4.2	4.2	4.2	4.2	4.2	0.0
Tau energy scale (shape)	$+0.29$ -0.22	$+0.22$ $+0.23$	$+0.82$ -0.63	$+0.42$ -0.75	$+0.63$ -0.31	0.0
$gg \to A$ acceptance	2.1	0.0	0.0	0.0	0.0	0.0
$bb \to A$ acceptance	3.6	0.0	0.0	0.0	0.0	0.0
MC Cross sections	0.0	2.2	2.2	10.0	6.0	0.0
QCD	0.0	0.0	0.0	0.0	0.0	15.0
Luminosity	5.8	0.0	5.8	5.8	5.8	0.0

TABLE II: Percentage systematic uncertainties for each distribution in the CDF $\tau_e\tau_{\rm had}$ analysis. Signal uncertainties are for $M_A = 130$ GeV.

Contribution	Signal	$Z \to \mu^+\mu^-$	$Z \to \tau\tau$	$t\bar{t}$	diboson	QCD
Jet energy scale (shape)	0.07	$+0.24$ -0.38	0.0	$+0.54$ -0.48	$+0.46$ -0.58	0.0
Muon identification	2.7	2.7	2.7	2.7	2.7	0.0
Tau identification	4.2	4.2	4.2	4.2	4.2	0.0
Tau energy scale (shape)	$+0.23$ -0.08	0.0	$+0.54$ -0.77	$+0.97$ -0.75	$+0.40$ -0.70	0.0
$gg \to A$ acceptance	2.1	0.0	0.0	0.0	0.0	0.0
$bb \to A$ acceptance	3.6	0.0	0.0	0.0	0.0	0.0
MC cross sections	0.0	2.2	2.2	10.0	6.0	0.0
QCD	0.0	0.0	0.0	0.0	0.0	20.0
Luminosity	5.8	0.0	5.8	5.8	5.8	0.0

TABLE III: Percentage systematic uncertainties for each distribution in the CDF $\tau_\mu\tau_{\rm had}$ analysis. Signal uncertainties are for $M_A = 130$ GeV.

Contribution	Signal	$Z \to e^+e^-$	$Z \to \mu^+\mu^-$	$Z \to \tau\tau$	$t\bar{t}$	diboson	QCD
Electron energy scale (shape)	$+0.23$ -0.46	0.0	-0.36 -0.60	$+0.72$ -0.62	0.00 $+0.26$	0.0	0.0
Jet energy scale (shape)	-0.08 0.00	0.0	-0.34 -0.30	-0.05 0.00	0.57	0.29	0.0
Electron identification	2.4	2.4	2.4	2.4	2.4	2.4	0.0
Muon identification	2.7	2.7	2.7	2.7	2.7	2.7	0.0
$gg \to A$ acceptance	2.1	0.0	0.0	0.0	0.0	0.0	0.0
$bb \to A$ acceptance	3.6	0.0	0.0	0.0	0.0	0.0	0.0
MC Cross sections	0.0	2.2	2.2	2.2	10.0	6.0	0.0
QCD	0.0	0.0	0.0	0.0	0.0	0.0	20.0
Luminosity	5.8	5.8	5.8	5.8	5.8	5.8	0.0

TABLE IV: Percentage systematic uncertainties for each distribution in the CDF $\tau_e\tau_\mu$ analysis. Signal uncertainties are for $M_A = 130$ GeV.

Contribution	Signal	diboson	QCD	$t\bar{t}$	$W \to l\nu$	$Z \to e^+ e^-$	$Z \to \tau\tau$
Electron Identification	3.3	3.3	0.0	3.3	3.3	3.3	3.3
Trigger (shape)	3.8	4.1	0.0	3.0	4.4	4.2	5.9
QCD	0.0	0.0	13.0	0.0	0.0	0.0	0.0
W+jets	0.0	0.0	0.0	0.0	6.8	0.0	0.0
Luminosity	6.1	6.1	0.0	6.1	6.1	6.1	6.1
Signal acceptance	4.0	0.0	0.0	0.0	0.0	0.0	0.0
Tau energy scale (shape)	0.4	0.0	0.0	0.0	0.0	0.0	1.3
Tau identification	6.0	5.3	0.0	7.1	5.6	3.9	4.1
Tau track reconstruction	1.0	1.0	0.0	1.0	1.0	1.0	1.0
electron-tau fake rate	0.0	0.0	0.0	0.0	0.0	13	0.0
MC cross sections	0.0	5.0	0.0	5.0	0.0	5.0	5.0

TABLE V: Percentage systematic uncertainties for each distribution in the DØ $\tau_e \tau_{\text{had}}$ analysis - combined across all three tau categories. Signal uncertainties are for $M_A = 130$ GeV.

Contribution	Signal	diboson	QCD	$t\bar{t}$	$W \to l\nu$	$Z \to \mu^+\mu^-$	$Z \to \tau\tau$
Luminosity	6.1	6.1	0.0	6.1	6.1	6.1	6.1
QCD	0.0	0.0	32	0.0	0.0	0.0	0.0
Trigger	3.0	3.0	0.0	3.0	3.0	3.0	3.0
W+jets	0.0	0.0	0.0	0.0	13.0	0.0	0.0
Muon identification	1.1	1.1	0.0	1.1	1.1	1.1	1.1
Signal acceptance	4.0	0.0	0.0	0.0	0.0	0.0	0.0
Tau energy scale (shape)	0.79	0.0	0.0	0.0	0.0	0.0	1.3
Tau identification	4.2	3.9	0.0	4.2	5.6	3.9	3.9
Tau track reco	1.0	1.0	0.0	1.0	1.0	1.0	1.0
MC cross sections	0.0	5.0	0.0	5.0	0.0	5.0	5.0

TABLE VI: Percentage systematic uncertainties for each distribution in the DØ $\tau_\mu \tau_{\text{had}}$ - (RunIIa) - combined across all three tau categories. Signal uncertainties are for $M_A = 130$ GeV.

Contribution	Signal	diboson	$Z \to \mu^+\mu^-$	$Z \to \tau\tau$	$t\bar{t}$	QCD
Luminosity	6.1	6.1	6.1	6.1	6.1	0.0
Trigger	5.0	5.0	5.0	5.0	5.0	0.0
Muon identification	4.0	4.0	4.0	4.0	4.0	0.0
Muon track reco	2.0	2.0	2.0	2.0	2.0	0.0
Signal acceptance	4.60	0.0	0.0	0.0	0.0	0.0
Tau identification	3.9	0.0	0.0	3.8	0.0	0.0
Tau track reconstruction	1.4	0.0	0.0	1.4	0.0	0.0
QCD	0.0	0.0	22	0.0	0.0	0.0
Tau energy scale	2.6	2.4	2.7	2.5	2.3	0.0
MC cross sections	0.0	5.0	5.0	5.0	5.0	5.0

TABLE VII: Percentage systematic uncertainties for each distribution in the DØ $\tau_\mu \tau_{\text{had}}$ - (RunIIb) - combined across all three tau categories. Signal uncertainties are for $M_A = 130$ GeV.

Contribution	Signal	QCD	$t\bar{t}$	$W \to l\nu$	diboson	$Z \to e^+e^-$	$Z \to \tau\tau$
Electron Identification	2.0	0.0	2.0	2.0	2.0	2.0	2.0
QCD	0.0	7.0	0.0	0.0	0.0	0.0	0.0
Trigger	4.0	0.0	4.0	4.0	4.0	4.0	4.0
Jet energy scale	2.0	0.0	2.0	2.0	2.0	2.0	2.0
Luminosity	6.1	0.0	6.1	6.1	6.1	6.1	6.1
Muon identification	0.40	0.0	0.40	0.40	0.40	0.40	0.40
Signal acceptance	4.0	0.0	0.0	0.0	0.0	0.0	0.0
MC cross sections	0.0	0.0	5.0	5.0	5.0	5.0	5.0
Vertx modelling	2.0	0.0	2.0	2.0	2.0	2.0	2.0

TABLE VIII: Percentage systematic uncertainties each distribution in the DØ $\tau_e\tau_\mu$ analysis. Signal uncertainties are for M_A = 130 GeV.

Mass / GeV	Observed Limits/*pb*	Expected Limits / pb				
		-2σ	-1σ	median	$+1\sigma$	$+2\sigma$
100	17.1	6.62	9.03	12.9	18.5	26.0
110	10.0	3.31	4.43	6.17	8.55	11.7
120	4.30	1.81	2.41	3.36	4.69	6.45
130	1.98	1.19	1.58	2.18	3.00	4.06
140	1.43	0.816	1.10	1.52	2.11	2.88
150	1.03	0.638	0.822	1.13	1.57	2.18
160	0.849	0.480	0.652	0.903	1.24	1.69
170	0.786	0.411	0.544	0.749	1.04	1.43
180	0.658	0.333	0.446	0.616	0.852	1.16
190	0.641	0.291	0.388	0.536	0.743	1.01
200	0.642	0.249	0.344	0.476	0.647	0.860

TABLE IX: Combined Cross section $\times$ branching ratio limits using Bayes method.

Mass / GeV	Observed Limits/*pb*	Expected Limits / pb				
		-2σ	-1σ	median	$+1\sigma$	$+2\sigma$
100	17.2	6.22	8.90	12.4	17.2	23.3
110	9.75	3.05	4.16	5.83	8.11	11.1
120	4.38	1.76	0.0	3.38	4.64	6.29
130	2.09	0.0	1.52	2.11	2.99	4.07
140	1.49	0.831	1.08	1.50	2.14	2.88
150	1.09	0.593	0.807	1.14	1.61	2.15
160	0.901	0.0	0.645	0.909	1.29	1.73
170	0.815	0.424	0.540	0.739	1.05	1.45
180	0.685	0.0	0.440	0.612	0.863	1.18
190	0.676	0.0	0.366	0.535	0.744	1.02
200	0.669	0.261	0.328	0.461	0.661	0.897

TABLE X: Combined cross section $\times$ branching ratio limits using CL_S. Zero's mark entries where limit setting jobs failed for technical reasons. These will be filled in once calculations have been completed.

IV. COMBINED RESULTS

Tables IX and X give the 95% confidence limits on the cross section $\times$ branching ratio for MSSM Higgs production and decay in the di-tau channel, using the two different approaches outlined above. Good agreement in the results for the two procedures is seen with variations at less than 10%. The results are shown graphically in Figure 3, where for each mass hypothesis the results were chosen from the limit setting method which gave the most conservative expected limit. The observed limits are generally in good agreement with expectation with no evidence for significant excess for $100 < M_A < 200$ GeV.

V. INTERPRETATION WITHIN THE MSSM

Though at leading order the Higgs sector of the MSSM can be described with just two parameters, with higher order corrections comes a dependence on other model parameters. To interpret the exclusion within the MSSM these parameters are fixed in four benchmark scenarios [22]. The four scenarios considered are defined in terms of: M_{SUSY}, the mass scale of squarks, μ, the Higgs sector bilinear coupling, M_2, the gaugino mass term, A_t, the trilinear coupling of the stop sector, A_b, the trilinear coupling of the sbottom sector and $m_{\tilde{g}}$ the gluino mass term. The maximal-mixing, m_h^{max}, scenario is defined as:
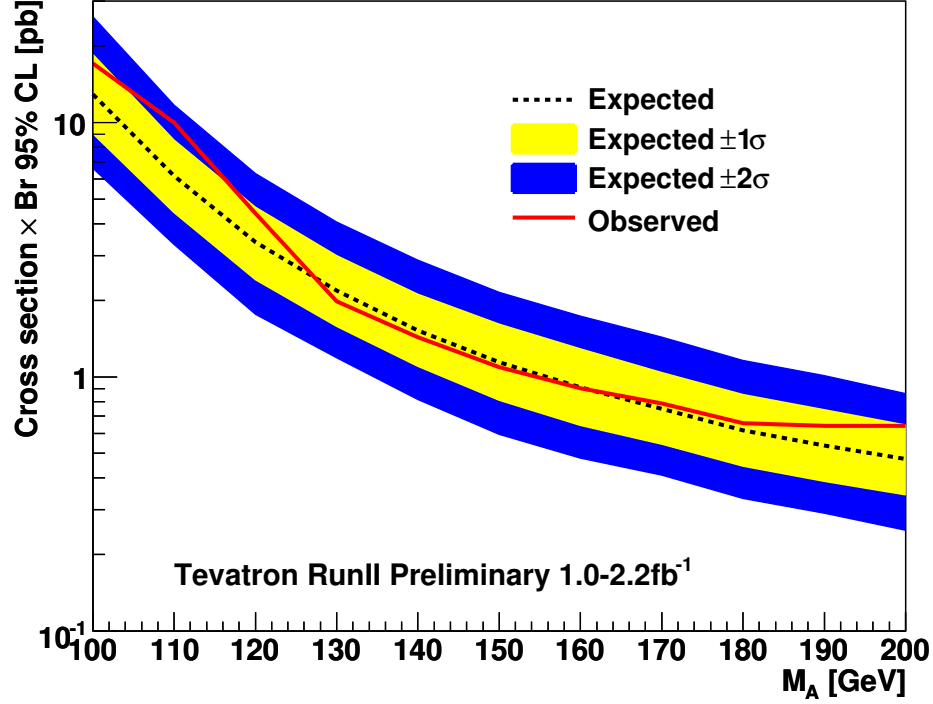
FIG. 3: 95% Confidence limits on cross section × branching ratio. The solid red and dashed black lines show the observed and expected limits respectively. The yellow and green shaded bands around the expected limit show the 1 and 2σ deviations from the expectation..

$$M_{\text{SUSY}} = 1\text{TeV}, \mu = 200 \text{ GeV}, M_2 = 200 \text{ GeV},$$
$$X_t = 2M_{\text{SUSY}}$$
$$A_b = A_t, m_{\tilde{g}} = 0.8M_{\text{SUSY}}.$$

and the no-mixing scenario - with vanishing mixing in the stop sector and a higher SUSY mass scale to avoid the LEP Higgs bounds:

$$M_{\text{SUSY}} = 2\text{TeV}, \mu = 200 \text{ GeV}, M_2 = 200 \text{ GeV},$$
$$X_t = 0, A_b = A_t, m_{\tilde{g}} = 0.8M_{\text{SUSY}}.$$

Four scenarios are constructed from these two by the consideration of both + and - signs for μ.

Tables XII, XI, XIV, and XIII give the observed and median expected 95% confidence limits on $\tan\beta$ for the tested mass hypotheses for the four different benchmark scenarios considered. This is shown graphically in Figure 4.

For this preliminary result the signal cross sections and branching fractions within each scenario have been calculated using FEYNHIGGS[21] with no theoretical uncertainties considered. Tanβ dependent width effects have not been included, though in the region of the tanβ-M_A plane where limits have been set these are not expected to strongly impact on the limit.

M_A GeV	Observed Limits	Expected Limits / pb				
		-2σ	-1σ	median	+1σ	+2σ
100	52	33	38	46	54	64
110	50	29	34	39	46	54
120	40	26	30	36	42	48
130	33	25	29	35	41	47
140	33	25	29	34	41	48
150	35	26	31	36	43	49
160	38	28	32	38	45	52
170	41	30	35	40	48	55
180	44	32	36	43	50	58
190	50	34	39	46	54	63
200	58	36	43	50	58	66

TABLE XI: Combined 95% confidence limits on tanβ for each mass hypothesis in the m_h max and negative μ scenario.

M_A GeV	Observed Limits	Expected Limits / pb				
		-2σ	-1σ	median	+1σ	+2σ
100	55	34	39	47	57	68
110	52	30	34	41	48	56
120	42	26	30	36	43	50
130	33	25	30	35	42	49
140	34	25	29	35	42	49
150	34	27	31	37	44	51
160	36	28	33	39	47	54
170	39	31	36	42	49	58
180	43	32	38	44	52	61
190	46	35	41	48	57	66
200	53	38	44	52	61	71

TABLE XII: Combined 95% confidence limits on tanβ for each mass hypothesis in the m_h max and positive μ scenario.

This is the first combination of Tevatron results from CDF and DØ in the $h \to \tau\tau$ channel and sets the most stringent limits to date on the search for MSSM Higgs in that final state. New results with increased luminosity and combining across channels (as recently demonstrated by DØ [23]) are expected soon and should be able to further improve the world's best limits on MSSM Higgs production.

M_A GeV	Observed Limits	Expected Limits / pb				
		-2σ	-1σ	median	+1σ	+2σ
100	53	33	39	46	55	65
110	50	29	33	40	47	55
120	41	26	30	36	42	49
130	33	25	29	35	41	48
140	34	26	30	35	42	49
150	36	26	31	37	43	50
160	38	28	32	38	46	53
170	42	30	35	41	48	56
180	45	32	37	43	51	59
190	51	35	40	47	54	64
200	59	37	43	51	59	67

TABLE XIII: Combined 95% confidence limits on tanβ for each mass hypothesis in the no-mixing and negative μ scenario.

M_A GeV	Observed Limits	Expected Limits / pb				
		-2σ	-1σ	median	+1σ	+2σ
100	54	34	39	47	56	66
110	51	29	34	40	47	55
120	41	26	30	36	42	49
130	33	25	29	35	41	48
140	35	26	30	36	42	49
150	36	27	31	37	44	51
160	39	28	33	39	46	53
170	42	31	35	41	49	57
180	45	32	37	44	51	60
190	52	35	40	47	56	65
200	60	37	44	51	60	69

TABLE XIV: Combined 95% confidence limits on tanβ for each mass hypothesis in the no-mixing and positive μ scenario.
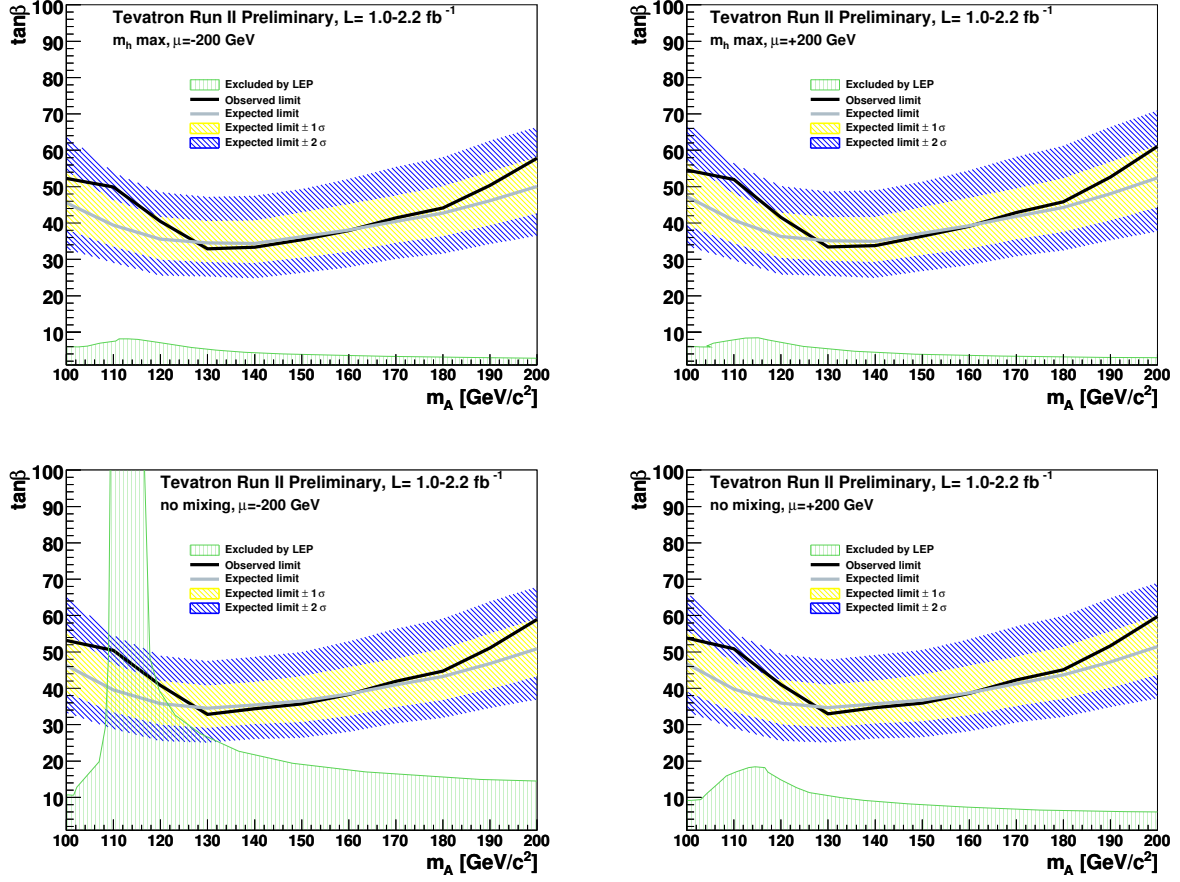
FIG. 4: 95% Confidence limits in the tanβ-M$_A$ plane for the 4 benchmark scenarios: maximal mixing (top) and no mixing (bottom) for $\mu < 0$ (left) and $\mu > 0$ (right). The black line denotes the observed limit, the grey line the expected limit and the hatched yellow and blue regions denote the ± 1 and $2\ \sigma$ bands around the expectation. The shaded light-green area shows the limits from LEP.

[1] H.P. Nilles, Phys. Rep. **110**, 1 (1984); H.E. Haber and G.L. Kane, Phys. Rep. **117**, 75 (1985).
[2] S. Schael *et al.* (The ALEPH, DELPHI, L3, and OPAL Collaborations), Eur. Phys. J. C **47**, 547 (2006).
[3] D. Acosta *et al.* (CDF Collaboration), Phys. Rev. D **71**, 032001 (2005).
[4] V.M. Abazov *et al.* (D0 Collaboration), Nucl. Instrum. Methods Phys. Res. A **565**, 463 (2006).
[5] CDF Collaboration, CDF Note 9071.
[6] V.M. Abazov *et al.* (D0 Collaboration), Phys. Rev. Lett. **101**, 071804 (2008).
[7] D0 Collaboration, D0 Note 5740-CONF.
[8] D0 Collaboration, D0 Note 5727-CONF.
[9] V.M. Abazov *et al.* (D0 Collaboration), Phys. Rev. Lett. **97**, 121802 (2006).
[10] A. Abulencia *et al.* (CDF Collaboration), Phys. Rev. Lett. **96**, 011802 (2006).
[11] T. Sjöstrand *et al.*, arXiv:hep-ph/0308153 (2003).
[12] J. Pumplin *et al.*, JHEP **0207**, 012 (2002).
[13] S. Jadech *et al.*, Comput. Phys. Commun. 76 (1993) 361
[14] E. Boos *et al.* (CompHEP Collaboration), Nucl. Instrum. Meth. A **534** (2004) 250.
[15] R. Brun and F. Carminati, CERN program library long writeup W5013 (1993). GEANT3 was used.
[16] M.L. Mangano *et al.*, JHEP 07, 001 (2003).
[17] CDF Collaboration, "Combined Upper Limit on Standard Model Higgs Boson Production for Winter 2009", CDF Conference Note 9674 (2009).
[18] DØ Collaboration, "Combined Upper Limits on Standard Model Higgs Boson Production from the DØ Experiment with up to 4.2 fb^{-1} of data" DØ Conferenve Note 9674 (2009).
[19] T. Junk, Nucl. Instrum. Meth. A **434** (1999) 435.; R. Barate *et al.*, Phys. Lett B **565** (2003).
[20] W. Fisher, FERMILAB-TM-2386-E (2007).
[21] S. Heinemeyer, W. Hollik, and G. Weiglein, Eur. Phys. J. C **9**, 343 (1999); Comput. Phys. Commun. **124**, 76 (2000); G. Degrassi *et al.*, Eur. Phys. J. C **28**, 133 (2003), M. Frank *et al.*, JHEP **0702**, 047 (2007). FEYNHIGGS version 2.6.3.
[22] M. Carena, S. Heinemeyer, C. E. M. Wagner, and G. Weiglein, Eur. Phys. J. C **45**, 797 (2006).
[23] D0 Collaboration, D0 Note 5935-CONF.